Inorg. Chem. **2006**, *45*, 2543–2552

Tri-$[Pt_2Tl]^{3-}$ and Polynuclear Chain $[Pt–Tl]_\infty^-$ Complexes Based on Nonbridged Pt^{II}–Tl^{I} Bonds: Solid State and Frozen Solution Photophysical Properties

Larry R. Falvello,[†] Juan Forniés,*[,†] Raquel Garde,[†] Ana García,[‡] Elena Lalinde,*[,‡] M. Teresa Moreno,[‡] Alexander Steiner,[§] Milagros Tomás,[†] and Isabel Usón*[†,∥]

Departamento de Química Inorgánica, Instituto de Ciencia de Materiales de Aragón, Universidad de Zaragoza-Consejo Superior de Investigaciones Científicas, 50009 Zaragoza, Spain, Departamento de Química-Grupo de Síntesis Química de La Rioja, UA-CSIC, Universidad de La Rioja, 26006, Logroño, Spain, ICREA at IBMB-CSIC, Departamento de Biología Estructural, Jordi Girona 18-26, 08034 Barcelona, Spain, and Department of Chemistry, University of Liverpool, Crown Street, Liverpool, L69 7ZD, U.K.

Received October 21, 2005

Treatment of $(NBu_4)_2[PtR_4]$ ($R = C_6F_5$) with 1 or 0.5 equiv of $TlNO_3$ in $EtOH/H_2O$ produces colorless crystals of trinuclear complex $(NBu_4)_3[Tl\{PtR_4\}_2]$, **1**, in which the Tl^+ center is complexed by two $[PtR_4]^{2-}$ fragments (Pt–Tl = 2.9777(4) and 3.0434(4) Å). The expected mixed complex with a Pt/Tl composition of 1:1, **2**, is generated as an orange microcrystalline solid by treating $[PtR_4]^{2-}$ with a large excess of $TlNO_3$ (∼8 equiv). Crystallographic analysis of **2** reveals the formation of a novel one-dimensional (1D) heterometallic linear chain $(NBu_4)_\infty[Tl\{PtR_4\}]_\infty$, **2**, formed by alternating a $[PtR_4]^{2-}$ fragment and a Tl^+ center with a uniform Pt–Tl bond separation along the chain of 3.0321(2) Å. Surprisingly, treatment of $(NBu_4)_2[PtR_4]$ with 1 equiv of $TlPF_6$ in EtOH yields pale greenish-yellow needles of an unusual adduct, $\mathbf{2}\cdot\{(NBu_4)(PF_6)\}_\infty$ (**3**), which was found to form a similar extended linear chain, $\{TlPtR_4\}_\infty$, constructed by two alternating Pt–Tl separations, a shorter (3.1028(6) Å) one and a longer (3.2306(6) Å) one. The solid state and solution photophysical properties have been examined. While complex **1** shows a high-energy MM′CT blue phosphorescence (450 nm), the extended chain in **2** exhibits a lower-energy emission (582 nm) than that in adduct **3** (505 nm). For products **2** and **3**, interesting luminescence thermochromism is observed in frozen solutions. The emissions are found to be strongly dependent on the solvent, concentration, and excitation wavelength.

Introduction

The synthesis of transition-metal-based supramolecules containing chromophoric molecules, conjugated molecules, or both has been extensively researched in recent years because of their potential application in molecular science.[1] Considerable effort has been directed toward the preparation of polymeric or supramolecular luminescent systems containing metals.[2] In particular, extended one-dimensional (1D) systems based on weak noncovalent (M···M, $\pi\cdots\pi$, or M···π) bonding interactions appear to be promising[1g,3] because the emissive properties of this type of aggregate has been shown to play a key role in molecular recognition; this is due to the dynamic nature of these weak contacts. Within

* To whom correspondence should be addressed. E-mail: juan.fornies@unizar.es (J.F.); elena.lalinde@dq.unirioja.es (E.L.).
† Universidad de Zaragoza-CSIC.
‡ Universidad de La Rioja, UA-CSIC.
§ University of Liverpool.
∥ ICREA at IBMB-CSIC.

(1) For recent reviews see: (a) Yam, V. W.-W.; Lo, W.-Y.; Lam, C.-H.; Fung, W. K.-M.; Wong, K. M.-C.; Lau, V. C.-Y.; Zhu, N. *Coord. Chem. Rev.* **2003**, *245*, 39. (b) Sun, S.-S.; Lees, A. J. *Coord. Chem. Rev.* **2002**, *230*, 170. (c) Fujita, M. *Chem. Soc. Rev.* **1998**, *27*, 417 and references therein. (d) Lehn, J. M. *Supramolecular Chemistry: Concepts and Perspectives*; VCH: Weinheim, Germany, 1995. (e) Hoeben, F. J. M.; Jonkheijm, P.; Meijer, E. W.; Schenning, A. P. H. J. *Chem. Rev.* **2005**, *105*, 1491. (f) Che, C.-M.; Lai, S.-W. *Coord. Chem. Rev.* **2005**, *249*, 1296. (g) Omary, M. A.; Mohamed, A. A.; Rawashdeh-Omary, M. A.; Fackler, J. P., Jr. *Coord. Chem. Rev.* **2005**, *249*, 1372. (h) Silverman, E. E.; Cardolaccia, T.; Zhao, X.; Kim, K.-Y.; Haskins-Glusac, K.; Shanze, K. S. *Coord. Chem. Rev.* **2005**, *249*, 1491. (i) Ren, T. *Organometallics* **2005**, *24*, 4854. (j) Chisholm, M. H.; Macintosh, A. M. *Chem. Rev.* **2005**, *105*, 2949. (k) Thanasekaran, P.; Liao, R.-T.; Liu, Y.-H.; Rajendran, T.; Rajagopal, S.; Lu, K.-L. *Coord. Chem. Rev.* **2005**, *249*, 1085. (l) Wong, W.-Y. *Coord. Chem. Rev.* **2005**, *249*, 971.

10.1021/ic051818u CCC: $33.50
Published on Web 02/14/2006

this field, linear chain systems based on square planar d^8 platinum complexes with short Pt···Pt distances, which show characteristic optical and electrical properties, have been extensively studied.[4] The stability of these structures is mainly the result of bonding interactions from the overlap of the $5d_z^2$ and $6p_z$ orbitals of the consecutive Pt^{II} centers in neutral, anionic, and cationic compounds being efficiently reinforced by electrostatic attraction in double-salt-type complexes.[5] Special interest is also currently devoted to the photophysics of discrete heteronuclear complexes stabilized by polar metal···metal bonds.[3a,6] However, compared to the numerous reports of hetero bi- and trimetallic complexes involving $Pt^{II} \rightarrow M$ donor acceptor bonds,[6a,7] the related extended mixed-metal systems containing unsupported platinum−metal bonds are scarce.[8] For compounds containing Pt−Tl bonds, since the luminescent discrete complex, *trans*-$[PtTl_2(CN)_4]$, was reported by Balch et al.,[9] several types of bi- ($Pt^{0,II}-Tl^{I}$, $Pt^{II}-Tl^{III}$),[10,12b] tri- ($Pt_2^{II,0}-Tl^{I}$, $Pt^{II}-Tl_2^{I}$, $Pt_2^{II}-Tl^{II}$),[11] and polynuclear complexes[12] have been structurally characterized. However, as far as we know, only two examples of polymeric Pt−Tl species[13] have been reported: an extended chain $\{$*trans*,*trans*,*trans*-$[PtTl_2R_2(C{\equiv}CtBu)_2]$-$(acetone)_2\}_x$ formed by octahedral "$PtTl_2R_2(C{\equiv}CtBu)_2$" fragments linked through weak alkynyl−thallium interactions[13a] and two polymorphs of the complex $[Tl^{I}(C_4H_9N_4)$-$Pt^{II}(CN)_2]$ (red and yellow), which differ in the nature of the metallophilic Pt····Tl interactions. Interestingly, the red form is a unique case where an extended ···Pt···Tl··· Pt···Tl··· chain, stabilized by unsupported metal−metal bonds, is produced.[13b]

In this paper we examine the reactivity of homoleptic $(NBu_4)_2[PtR_4]$ toward Tl^{I}. We report the synthesis and unusual properties of two different anionic $[Pt-Tl]^-_\infty$ chain systems, $(NBu_4)_\infty[Tl\{PtR_4\}]_\infty$, **2**, with a regular Pt−Tl interaction and an unusual adduct **2**·$\{(NBu_4)(PF_6)\}_\infty$, **3**, displaying two different Pt−Tl separations, together with

(2) (a) Liu, Y.; Li, Y.; Schanze, K. S. *J. Photochem. Photobiol., C* **2002**, *3*, 1 and references given therein. (b) Seward, C.; Jia, W.-L.; Wang, R.-Y.; Enright, G. D.; Wang, S. *Angew. Chem., Int. Ed. Engl.* **2004**, *43*, 2933 and references given therein. (c) Lefebvre, J.; Batchelor, R. J.; Leznoff, D. B. *J. Am. Chem. Soc.* **2004**, *126*, 16117. (d) Fernández, E. J.; Laguna, A.; López de Luzuriaga, J. M.; Montiel, M.; Olmos, M. E.; Pérez, J. *Organometallics* **2005**, *24*, 1631 and references therein. (e) Dequeant, M. Q.; McGuire, R., Jr.; McMillin, D. R.; Ren, T. *Inorg. Chem.* **2005**, *44*, 6521.

(3) (a) Gade, L. H. *Angew. Chem., Int. Ed. Engl.* **2001**, *40*, 3573 and references given therein. (b) Fung, E. Y.; Olmstead, M. M.; Vickery, J. C.; Balch, A. L. *Coord. Chem. Rev.* **1998**, *171*, 151. For some recent examples, see: (c) Lu, W.; Chan, M. C. W.; Zhu, N.; Che, C.-M.; He, Z.; Wong, K.-Y. *Chem.−Eur. J.* **2003**, *9*, 6155 and references given therein. (d) Willison, S. A.; Jude, H.; Antonelli, R. M.; Rennekamp, J. M.; Eckert, N. A.; Bauer, J. A. K.; Connick, W. B. *Inorg. Chem.* **2004**, *43*, 2548. (e) Haneline, M. R.; Tsunoda, M.; Gabbai, F. P. *J. Am. Chem. Soc.* **2002**, *124*, 3737. (f) Hayashi, A.; Olmstead, M. M.; Attar, S.; Balch, A. L. *J. Am. Chem. Soc.* **2002**, *124*, 5791. (g) Ara, I.; Forniés, J.; Gómez, J.; Lalinde, E.; Moreno, M. T. *Organometallics* **2000**, *19*, 3137. (h) Coker, N. L.; Bauer, J. A. K.; Elder, R. C. *J. Am. Chem. Soc.* **2004**, *126*, 12. (i) Fernández, E. J.; López de Luzuriaga, J. M.; Monge, M.; Montiel, M.; Olmos, M. E.; Pérez, J.; Laguna, A.; Mendizabal, F.; Mohamed, A. A.; Fackler, J. P., Jr. *Inorg. Chem.* **2004**, *43*, 3573. (j) Lee, Y.-A.; McGarrah, J. E.; Lachicotte, R. J.; Eisenberg, R. *J. Am. Chem. Soc.* **2002**, *124*, 10662. (k) White-Morris, R. L.; Olmstead, M. M.; Jiang, F.; Tinti, D. S.; Balch, A. L. *J. Am. Chem. Soc.* **2002**, *124*, 2327. (l) Rawashdeh-Omary, M. A.; Omary, M. A.; Patterson, H. H.; Fackler, J. P., Jr. *J. Am. Chem. Soc.* **2001**, *123*, 11237. (m) Dias, H. V. R.; Diyabalanage, H. V. K.; Eldabaja, M. G.; Elbjeirami, O.; Rawashdeh-Omary, M. A.; Omary, M. A. *J. Am. Chem. Soc.* **2005**, *127*, 7489 and references therein. (n) Wang, S.; Fackler, J. P.; King, C.; Wang, J. C. *J. Am. Chem. Soc.* **1988**, *110*, 3308.

(4) (a) Gliemann, G.; Yersin, H. *Struct. Bonding* **1985**, *62*, 87. (b) Houlding, V. H.; Miskowski, V. M. *Coord. Chem. Rev.* **1991**, *111*, 145. For recent examples, see: (c) Fontana, M.; Chanzy, H.; Caseri, W. R.; Smith, P.; Schenning, A. P. H. J.; Meijer, E. W.; Gröhn, F. *Chem. Mater.* **2002**, *14*, 1730. (d) Lai, S. W.; Lam, H.-W.; Lu, W.; Cheung, K.-K.; Che, C.-M. *Organometallics* **2002**, *21*, 226 and references given therein. (e) Goshe, A. J.; Steel, I. M.; Bosnich, B. *J. Am. Chem. Soc.* **2003**, *125*, 444. (f) Buss, C. E.; Anderson, C. E.; Pomije, M. K.; Luzt, C. M.; Britton, D.; Mann, K. R. *J. Am. Chem. Soc.* **1998**, *120*, 7783. (g) Drew, S. M.; Janzen, D. E.; Buss, C. E.; McEwan, D. I.; Dublin, K. M.; Mann, K. R. *J. Am. Chem. Soc.* **2001**, *123*, 8414. (h) Yam, V. W.-W.; Wong, K. M.-C.; Zhu, N. *J. Am. Chem. Soc.* **2002**, *124*, 6506. (i) Arena, G.; Calogero, G.; Campagna, S.; Scolaro, L. M.; Ricevuto, V.; Romeo, R. *Inorg. Chem.* **1998**, *37*, 2763. (j) Buss, C. E.; Mann, K. R. *J. Am. Chem. Soc.* **2002**, *124*, 1031.

(5) (a) Novoa, J. J.; Aullón, G.; Alemany, P.; Alvarez, S. *J. Am. Chem. Soc.* **1995**, *117*, 7169. (b) Caseri, W. R.; Chanzy, H. D.; Feldman, K.; Fontana, M.; Smith, P.; Tervoort, T. A.; Goossens, J. G. P.; Meijer, E. W.; Schemmomg, A. P. H. J.; Dolbnya, I. P.; Debije, M. G.; de Haas M. P.; Warman, J. M.; van de Craats, A. M.; Friend, R. H.; Sirringhaus, H.; Stutzmann, N. *Adv. Mater.* **2003**, *15*, 125.

(6) (a) Pyykkö, P. *Chem. Rev.* **1997**, *97*, 597. (b) Forniés, J.; Ibáñez, S.; Martín, A.; Gil, B.; Lalinde, E.; Moreno, M. T. *Organometallics* **2004**, *23*, 3963 and references given therein. (c) Wei, Q.-H.; Yin, G.-Q.; Zhang, L.-Y.; Shi, L.-X.; Mao, Z.-W.; Chen, Z.-N. *Inorg. Chem.* **2004**, *43*, 3484. (d) Casado, M. A.; Pérez-Torrente, J. J.; López, J. A.; Ciriano, M. A.; Lahoz, F. J.; Oro, L. A. *Inorg. Chem.* **1999**, *38*, 2482 and references given therein. (e) Balch, A. L.; Catalano, V. J.; Chatfield, M. A.; Nagle, J. K.; Olmstead, M. M.; Reedy, P. E., Jr. *J. Am. Chem. Soc.* **1991**, *113*, 1252. (f) Catalano, V. J.; Malwitz, M. A. *J. Am. Chem. Soc.* **2004**, *126*, 6560. See also ref 11c.

(7) (a) Forniés, J.; Martín, A. In *Metal Clusters in Chemistry*; Braunstein, P., Oro, L. A., Raithby, P. R., Eds.; Wiley-VCH: Weinheim, Germany, 1999; Vol. 1, pp 417−443. (b) Alonso, E.; Forniés, J.; Fortuño, C.; Martín, A.; Orpen, A. G. *Organometallics* **2003**, *22*, 5011 and references given therein. (c) Liu, H.; Tan, A. L.; Cheng, C. R.; Mok, K. F.; Hor, T. S. A. *Inorg. Chem.* **1997**, *36*, 2916.

(8) (a) Stender, M.; White-Morris, R. L.; Olmstead, M. M.; Balch, A. L. *Inorg. Chem.* **2003**, *42*, 4504. (b) Stork, J. R.; Rios, D.; Pham, D.; Bicocca, V.; Olmstead, M. M.; Balch, A. L. *Inorg. Chem.* **2005**, *44*, 3466.

(9) (a) Nagle, J. K.; Balch, A. L.; Olmstead, M. M. *J. Am. Chem. Soc.* **1988**, *110*, 319. (b) Weissbart, B.; Balch, A. L.; Tinti, D. S. *Inorg. Chem.* **1993**, *32*, 2096.

(10) Binuclear Pt−Tl systems: (a) Balch, A. L.; Rowley, S. P. *J. Am. Chem. Soc.* **1990**, *112*, 6139. (b) Balch, A. L.; Yung, E. Y.; Nagle, J. K.; Olmstead, M. M.; Rowley, S. P. *Inorg. Chem.* **1993**, *32*, 3295. (c) Catalano, V. J.; Bennett, B. L.; Muratidis, S.; Noll, B. C. *J. Am. Chem. Soc.* **2001**, *123*, 173. (d) Oberbeckmann-Winter, N.; Braunstein, P.; Welter, R. *Organometallics* **2004**, *23*, 6311. (e) Ma, G.; Kritikos, M.; Glaser, J. *Eur. J. Inorg. Chem.* **2001**, 1311. (f) Ma, G.; Fischer, A.; Glaser, J. *Eur. J. Inorg. Chem.* **2002**, 1307. (g) Ma, G.; Kritikos, M.; Maliarik, M.; Glaser, J. *Inorg. Chem.* **2004**, *43*, 4328.

(11) Trinuclear complexes: (a) Renn, O.; Lippert, B.; Multikainen, I. *Inorg. Chim. Acta* **1993**, *208*, 219. (b) Usón, R.; Forniés, J.; Tomás, M.; Garde, R. *J. Am. Chem. Soc.* **1995**, *117*, 1837. (c) Catalano, V. J.; Bennett, B. L.; Yson, R. L.; Noll, B. C. *J. Am. Chem. Soc.* **2000**, *122*, 10056. (d) Song, H.-B.; Zhang, Z.-Z.; Hui, Z.; Che, C.-M.; Mak, T. C. W. *Inorg. Chem.* **2002**, *41*, 3146. (e) ($PtTl_2$) Quadrelli, E. A.; Davies, J. E.; Johnson, B. F. G.; Feeder, N. *Chem. Commun.* **2000**, 1031 (Pt−Tl = 3.2393(15) Å).

(12) Polynuclear Pt−Tl complexes: (a) Ezomo, O. J.; Mingos, D. M. P.; Williams, I. D.; *J. Chem. Soc., Chem. Commun.* **1987**, 924. (b) Usón, R.; Forniés, J.; Tomás, M.; Garde, R.; Merino, R. I. *Inorg. Chem.* **1997**, *36*, 1383. (c) Spivak, G. J.; Vittal, J. J.; Pudephatt, R. J. *Inorg. Chem.* **1998**, *37*, 5474. (d) Berenguer, J. R.; Forniés, J.; Gómez, J.; Lalinde, E.; Moreno, M. T. *Organometallics* **2001**, *20*, 4847. (e) Stadnichenko, R.; Sterenberg, B. T.; Bradford, A. M.; Jennings, M. C.; Puddephatt, R. J. *J. Chem. Soc., Dalton Trans.* **2002**, 1212. (f) Devic, T.; Batail, P.; Fourmigué, M.; Avarvari, N. *Inorg. Chem.* **2004**, *43*, 3136. (g) Chartmant, J. P. H.; Forniés, J.; Gómez, J.; Lalinde, E.; Merino, R. I.; Moreno, M. T.; Orpen, A. G. *Organometallics* **2003**, *22*, 652.

(13) (a) Ara, I.; Berenguer, J. R.; Forniés, J.; Gómez, J.; Lalinde, E.; Merino, R. I. *Inorg. Chem.* **1997**, *36*, 6461. (b) Stork, J. R.; Olmstead, M. M.; Balch, A. L. *J. Am. Chem. Soc.* **2005**, *127*, 6512.

trimetallic $(NBu_4)_3[Tl\{PtR_4\}_2]$, **1**, which can be regarded as a fragment of the extended structure.

Experimental Section

The reactions were performed under an Ar atmosphere, and the solvents were purified by standard methods. C, H, and N analyses, conductivities, and IR, mass, and NMR spectroscopies were performed as described elsewhere.[12g] UV−vis spectra were recorded on a Hitachi U-3400 spectrometer. Excitation and emission spectra were obtained on a Perkin-Elemer luminescence spectrometer LS 50B and on a Jobin-Yvon Horiba Fluorolog 3 model FL3-11 spectrofluorimeter, in which the lifetime measurements were performed operating in the phosporimeter mode (with a F1-1029 lifetime emission PMT assembly, using a 450 W Xe lamp). $(NBu_4)_2[Pt(C_6F_5)_4]$ was prepared by literature method.[14]

Preparation of $(NBu_4)_3[Tl\{Pt(C_6F_5)_4\}_2]$, 1. $TlNO_3$ (0.016 g, 0.061 mmol) was added to a suspension of $(NBu_4)_2[Pt(C_6F_5)_4]$ (0.164 g, 0.122 mmol) (1:2 molar ratio) in EtOH/H_2O (12/5 mL) at room temperature. After the mixture was stirred for 3 h, the resulting white suspension was filtered. The white solid obtained was washed with water and air-dried (0.148 g, 92% yield). Anal. Calcd for $C_{96}F_{40}H_{108}N_3Pt_2Tl$: C, 43.37; H, 4.09; N, 1.58. Found: C, 43.19; H, 3.97; N, 4.09. MS: (ES+) *m*/*z* 242 $[NBu_4]^+$ 100%; (ES−) *m*/*z* 1067 $[PtTl(C_6F_5)_4]^-$ 24%, 863 $[Pt(C_6F_5)_4]^-$ 8%, 696 $[Pt(C_6F_5)_3]^-$ 100%. IR (KBr, cm^{-1}): $\nu(C_6F_5)$ 1495 (s), 1446 (s), 1051 (s), 1040 (sh), 950 (s), 766 (s); $\nu(NBu_4)$ 880 (m). Λ_M: (5×10^{-4} M acetone solution) 253 Ω^{-1} cm^2 mol^{-1}; (5×10^{-4} M acetonitrile solution) 308 Ω^{-1} cm^2 mol^{-1}. ^1H NMR (300.1 MHz, $CDCl_3$): δ 3.20 (m), 1.66 (m), 1.41 (sext), 0.97 (t) (NBu_4). ^{19}F NMR (282.4 MHz, $CDCl_3$): δ (323 K) −115.2 (s br, $J_{o-F-Pt} \approx$ 260 Hz, 2*o*-F), −166.9 (s br, *p*-F + 2*m*-F); (298 K) −115.2 (s br, 2*o*-F), −166.6 (*p*-F + 2*m*-F). The *o*-F signals become broader, upon cooling, and finally resolve at 223 K in a broad doublet at ca. −115.0 ($J_{o-F-^{203,205}Tl} \approx$ 3530 Hz, 2*o*-F) ($T_{coalescence}$ = 233−243 K) and a broad singlet at −115.3. The *p*-F and *m*-F signals also resolve in four different broad signals (−163.8, −164.8, −167.2, −168.5). In acetone-d_6 at 298 K, there are peaks at −113.5 ($^3J_{o-F-Pt}$ = 332 Hz, 2*o*-F), −167.6 (m, 2*m*-F), and −168.6 ppm (1*p*-F), and at 193 K, there are peaks at −112.1 (d br, $^3J_{o-F-Tl} \approx$ 3470 Hz, *o*-F), −113.0 (s br, *o*-F), −166.1, −167.1, and −167.9 ppm (br, *p*-F + 2*m*-F).

Preparation of $(NBu_4)_\infty[Tl\{Pt(C_6F_5)_4\}]_\infty$, 2. A colorless solution formed by $(NBu_4)_2[Pt(C_6F_5)_4]$ (0.357 g, 0.265 mmol) and $TlNO_3$ (0.575 g, 2.158 mmol) (1:8 molar ratio) in DMSO (5 mL) was stirred for 15 min. Then, EtOH (20 mL) and H_2O (12 mL) were added, and slow evaporation (24 h) of the solution yielded an orange microcrystalline solid which was filtered, washed with water, and air-dried (0.307 g, 88% yield). Anal. Calcd for $C_{36}F_{20}H_{36}NPtTl$: C, 36.67; H, 2.77; N, 1.07. Found: C, 36.93; H, 2.99; N, 1.00. MS: (ES+) *m*/*z* 242 $[NBu_4]^+$ 100%; (ES−) *m*/*z* 1067 $[PtTl(C_6F_5)_4]^-$ 16%, 696 $[Pt(C_6F_5)_3]^-$ 100%. IR (KBr, cm^{-1}): $\nu(C_6F_5)$ 1480 (s), 1443 (s), 1427 (sh), 1052 (s), 1041(sh), 946 (s), 770 (s); $\nu(NBu_4)$ 880 (m). Λ_M: (5×10^{-4} M acetone solution) 95 Ω^{-1} cm^2 mol^{-1}; (5×10^{-4} M acetonitrile solution) 100 Ω^{-1} cm^2 mol^{-1}. ^1H NMR (300.1 MHz, $CDCl_3$): δ 3.13 (m), 1.62 (m), 1.39 (sext), 0.97 (t) (NBu_4). ^{19}F NMR (282.4 MHz, $CDCl_3$): δ (323 K) ∼ −115.3 (d br, $J_{o-F-Tl} \approx$ 1700 Hz, 2*o*-F), −164.6 (s br, *p*-F), −165.2 (s br, 2*m*-F); (298 K) ∼ −115.2 ($J_{o-F-Tl} \approx$ 1720 Hz, 2*o*-F), −164.4 (s br, *p*-F), −165.0 (s br, 2*m*-F). The broad doublet of 2*o*-F vanishes at ca. 258 K and resolves into two different signals at low temperature (223 K): δ −114.9 ($^3J_{o-F-Pt}$ = 315 Hz), −115.2 (d br, $^1J_{F-Tl} \approx$ 3595 Hz). The signal from 2*m*-F also splits ($T_{coalescence} \approx$ 238 K) at 258 K, and one of the signals coincides with that of *p*-F: −163.7 (*p*-F + 1*m*-F), −164.8 (1*m*-F). The ΔG^*_{258} for the *o*-F signals is ca. 52 kJ/mol. In acetone-d_6 at 298 K, there are peaks at −113.5 (d br, 2*o*-F) and −166.4 ppm (m, *p*-F + 2*m*-F).

Preparation of $(NBu_4)_\infty[Tl\{Pt(C_6F_5)_4\}]_\infty \cdot \{(NBu_4)(PF_6)\}_\infty$, 3. A white suspension formed by $(NBu_4)_2[Pt(C_6F_5)_4]$ (0.135 g, 0.100 mmol) in absolute EtOH (10 mL) was treated with $TlPF_6$ (0.035, 0.100 mmol), and the mixture was stirred for 30 min. The resulting colorless solution was filtered through Celite and was left open to air. After ca. 3 days, large greenish-yellow needle-shaped crystals of **2**·$\{(NBu_4)(PF_6)\}_\infty$ (**3**) crystallized (0.095 g, 56% yield). Anal. Calcd for $C_{56}F_{26}H_{72}N_2PPtTl$: C, 39.62; H, 4.28; N, 1.65. Found: C, 39.46; H, 4.00; N, 1.68. MS: (ES+) *m*/*z* 242 $[NBu_4]^+$ 100%; (ES−) *m*/*z* 1067 $[PtTl(C_6F_5)_4]^-$ 73%, 696 $[Pt(C_6F_5)_3]^-$ 36%. IR (KBr, cm^{-1}): $\nu(C_6F_5)$ 1053 (s), 1041 (sh), 947 (s), 740 (s); $\nu(NBu_4)$ 882 (s); $\nu(PF_6)$ 770 (m). Λ_M: (5×10^{-4} M acetone solution) 228 Ω^{-1} cm^2 mol^{-1}; (5×10^{-4} M acetonitrile solution) 224 Ω^{-1} cm^2 mol^{-1}. ^1H NMR (300.1 MHz, $CDCl_3$): δ 3.14 (m); 1.61 (m); 1.40 (sext); 0.98 (t) (NBu_4). ^{19}F NMR (282.4 MHz, $CDCl_3$): the signals for the C_6F_5 groups of this adduct at different temperatures are identical to those for **2** (see Figure 1). In the spectra, an additional signal from PF_6^- is observed (δ −111.5, $^1J_{F-P}$ = 190 Hz).

X-ray Crystallography. Crystal data and other details of the structure analyses are presented in Table 1. Colorless crystals of **1** were obtained by slow diffusion of *n*-hexane into a dichloromethane solution at room temperature; while orange crystals of **2** and pale greenish-yellow crystals (needles) of **3** were obtained by leaving ethanol solutions of these complexes to evaporate at room temperature. The diffraction measurements of **1** and **3** were made on a NONIUS κ-CCD area-detector diffractometer, using graphite-monochromated Mo Kα radiation. Images were processed using the DENZO and SCALEPACK suite of programs.[15] The structure of **1** was solved by Patterson and Fourier methods using the DIRDIF92 program,[16] and the absorption correction was performed using SORTAV.[17] The structure of **3** was solved by direct methods using the SHELXS-97 program,[18] and the absorption correction was performed using MULTISCAN.[17] The structures were refined by full-matrix least squares on F^2 with SHELXL-97.[19] All non-hydrogen atoms were assigned anisotropic displacement parameters, and all hydrogen atoms were constrained to idealized geometries fixing isotropic displacement parameters of 1.2 times the U_{iso} value of their attached carbon for CH_2 hydrogens and 1.5 for the methyl groups. For both structures, part of the NBu_4^+ was modeled adequately. There are peaks of electron density bigger than 1 e $Å^{-3}$ in the final map, but they are located very close to the platinum and thallium atoms and have no chemical meaning.

Intensity data for complex **2** were gathered using a Stoe AED4 automated four-circle diffractometer.[20] Absorption corrections were

(14) Usón, R.; Forniés, J.; Martínez, F.; Tomás, M. *J. Chem. Soc., Dalton Trans.* **1980**, 888.

(15) Otwinowski, Z.; Minor, W. In *Methods in Enzymology*; Carter, C. V., Jr., Sweet, R. M., Eds.; Academic Press: New York, 1997; Vol. 276A, p 307.

(16) Beursken, P. T.; Beursken, G.; Bosman, W. P.; de Gelder, R.; García-Granda, S.; Gould, R. O.; Smith, J. M. M.; Smykalla, C. *The DIRDIF92 Program System*; Technical Report of the Crystallography Laboratory; University of Nijmegen: Nijmegen, The Netherlands, 1992.

(17) Blessing, R. H. *Acta Crystallogr.* **1995**, *A51*, 33.

(18) Sheldrick, G. M. *SHELXS97*: *Program for the Solution of Crystal Structures*; University of Göttingen: Göttingen, Germany, 1997.

(19) Sheldrick, G. M. *SHELXL97*: *Program for Crystal Structure Refinement*; University of Göttingen: Göttingen, Germany, 1997.

(20) (a) AED-4 control program: DIF4 (Stoe & Cie. GmbH. Darmstadt, Germany). (b) AED-4 data reduction: REDU4 Rev. 7.03. (Stoe & Cie. GmbH. Darmstadt, Germany).

Table 1. Crystal Data and Structure Refinement Details for **1**, **2**, and **3**

	1	**2**	**3**
empirical formula	$C_{96}H_{108}F_{40}N_3Pt_2Tl$	$C_{40}H_{36}F_{20}PtTl$	$C_{56}H_{72}F_{26}N_2PPtTl$
fw	2658.40	1310.16	1697.59
temp (K)	173(1)	180(1)	173(1)
wavelength (Å)	0.71073	0.71073	0.71073
cryst syst	monoclinic	hexagonal	orthorhombic
space group	$P2_1/n$	$P6_222$	$Pcaa$
a (Å), α (deg)	17.6450(2), 90	14.2476(7), 90	12.6668(2), 90
b (Å), β (deg)	22.8355(2), 99.67	14.2476(7), 90	14.2938(3), 90
c (Å), γ (deg)	26.0284(3), 90	18.1828(11), 120	35.0539(9), 90
V (Å^3), Z	10338.58(19), 4	3198.3(3), 3	6346.7(2), 4
calcd density (Mg/m^3)	1.708	2.041	1.777
abs coeff (μ) (mm^{-1})	4.372	7.169	4.877
F(000)	5208	1866	3320
cryst size (mm^3)	0.35 × 0.25 × 0.15	*a*	0.60 × 0.15 × 0.10
2θ range (deg)	1.30−27.52	2.78−25.00	2.23−27.90
index ranges	$-22 \le h \le 22$	$0 \le h \le 14$	$-16 \le h \le 16$
	$-29 \le k \le 29$	$0 \le k \le 14$	$-18 \le k \le 18$
	$-33 \le l \le 33$	$-21 \le l \le 21$	$-46 \le l \le 46$
no. reflns collected	157 093	4241	56 659
independent refls	23724 (R(int) = 0.1284)	1893 (R(int) = 0.0553)	7423 (R(int) = 0.0670)
data/restraints/params	23 724/3/1171	1893/140/131	7423/5/363
GOF on F^2[b]	1.034	1.014	1.020
final R indices [$I > 2\sigma(I)$][b]	R1 = 0.0605, wR2 = 0.1166	R1 = 0.0580, wR2 = 0.1119	R1 = 0.0568, wR2 = 0.1495
R indices (all data)[b]	R1 = 0.1443, wR2 = 0.1433	R1 = 0.1766, wR2 = 0.1501	R1 = 0.1315, wR2 = 0.1870
largest diff. peak and hole	1.546 and −1.305 e Å^{-3}	0.950 and −0.625 e Å^{-3}	1.251 and −1.332 e Å^{-3}

[a] Unfortunately, the crystal was lost before its dimensions could be measured. [b] $R1 = \sum(|F_o| - |F_c|)/\sum|F_o|$; $wR2 = [\sum w(F_o^2 - F_c^2)^2/\sum wF_o^2]^{1/2}$; $GOF = \{\sum[w(F_o^2 - F_c^2)^2]/(N_{obs} - N_{params})\}^{1/2}$; $w = [\sigma^2(F_o^2) + (g_1P)^2 + g_2P]^{-1}$; $P = [\max(F_o^2;0) + 2F_c^2]/3$.

applied using ψ scans. The concentration of a large fraction of the scattering density into just two independent atoms, Pt and Tl, produced a pseudosymmetry that required special procedures in data collection and structure solution. For data collection, the reflections with $l = 6n$, resulting form the special location of both kinds of heavy atoms on the c axis, at $z = n/6$ sites were measured in one batch, while all other reflections were measured separately and much more slowly. For the structure solution, while the Pt and Tl atoms were located without any problem, the NBu_4^+ cations and C_6F_5 ligands did not appear in conventional difference maps. These groups were revealed in difference maps in which the value of F_o^2 for all intense reflections had been scaled down by a factor of 10 and in which the values of F_c were calculated with a lighter scatterer (Cu) at the heavy atom positions.[21] Once all atoms had been located, it was possible to refine the structure successfully in least-squares calculations involving both restraints and constraints for the lighter atoms. The proportion of the two possible absolute structures cannot be established from the diffraction data.

Results and Discussion

Synthesis and Characterization. Treatment of a suspension of $(NBu_4)_2[Pt(C_6F_5)_4]$ in EtOH with 1 or 0.5 equiv of $TlNO_3$ results in the immediate formation of the trinuclear anionic complex $(NBu_4)_3[Tl\{PtR_4\}_2]$, **1**, as a white precipitate. The complex of stoichiometry of Pt/Tl (1:1) was prepared by allowing $(NBu_4)_2[Pt(C_6F_5)_4]$ to react in DMSO (∼5 mL) with an excess of $TlNO_3$ (∼1:8). EtOH/H_2O was added to the resulting colorless solution, and the mixture was allowed to stand without disturbance. Orange microcrystalline needles of $(NBu_4)_\infty[Tl\{PtR_4\}]_\infty$, **2**, were obtained in high yield (88%). Surprisingly, slow evaporation of a colorless ethanolic solution of $(NBu_4)_2[PtR_4]$ and $TlPF_6$ (1:1 molar ratio) yielded greenish-yellow needles of a cocrystallization adduct **2**·$\{(NBu_4)(PF_6)\}_\infty$, **3** (56%). With the goal of preparing another adduct of complex **2**, we mixed $(NBu_4)_2[PtR_4]$ with 1 equiv of Tl(acac) in EtOH, but in this case, only colorless crystals of **1** were formed. All three complexes, **1**−**3**, gave satisfactory elemental analyses, and their mass spectra (ES−) reveal the presence of a peak at m/z 1067 corresponding to the bimetallic anion $[TlPtR_4]^-$ as the only heterometallic species. The values of the conductivity measurements in acetonitrile solution found for complexes **1**−**3** are 308 (**1**), 100 (**2**), and 224 (**3**) Ω^{-1} cm^2 mol^{-1}, respectively. Support for the presence of the Pt−Tl bond in **2** and **3** is inferred from ^{19}F NMR spectroscopy. The NMR data and behavior of both complexes are identical in solution, and they indicate that the extended chain dissociates mainly in discrete binuclear fragments. As an illustration of this, the variable-temperature ^{19}F NMR spectra in the *o*-fluorine region of **3** is shown in Figure 1.

As expected, only one set of C_6F_5 signals is seen. At low temperature (223 K) the pattern is that expected for a rigid $[TlPtR_4]^-$ fragment with the Tl center interacting with the four endo *o*-fluorine atoms, one from each static C_6F_5 ring, giving rise to two distinct *o*-fluorine and *m*-fluorine (endo and exo) resonances. The endo *o*-fluorine atoms appear as a broad doublet centered at ca. −115.2 ppm exhibiting a thallium−fluorine coupling $J_{o-F-^{203,205}Tl}$ of ca. 3595 Hz, which is comparable to those observed in other compounds with F···Tl bonding contacts.[12g,22] The exo *o*-fluorine atoms are seen as a broad singlet at δ −114.9 with platinum satellites ($^3J_{F-^{195}Pt} \approx 315$ Hz). Increasing the monitoring temperature resulted in a clear broadening of both the exo and endo fluorine resonances, which coalesce at about 258 K in the *o*-fluorine region ($\Delta G^*_{258} \approx 52$ kJ/mol) and at ∼238 K in

(21) Usón, I.; Steiner, A.; Tomás, M.; Ara, I. *Abstracts of the Annual Meeting of the American Crystallographic Association*; American Crystallographic Association: Buffalo, NY, 1995; M172.

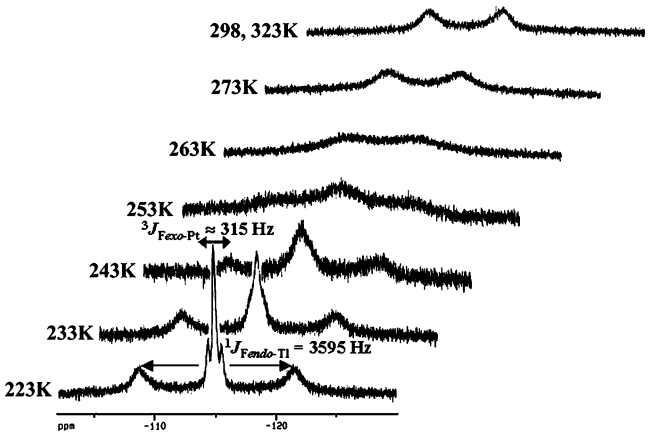

Figure 1. Variable-temperature ^{19}F NMR spectra in $CDCl_3$ in the *o*-fluorine region of $(NBu_4)_\infty[Tl\{Pt(C_6F_5)_4\}]_\infty \cdot \{(NBu_4)PF_6\}_\infty$, **3**.

the meta region. As is observed in Figure 1, the exchange of the *o*-fluorine signals gives rise to one broad doublet with an averaged thallium fluorine coupling of ca. 1700 Hz at higher temperatures. This pattern confirms the presence of the $[TlPtR_4]^-$ fragment in solution (even at 323 K), and the observed equilibration of the endo and exo *o*-fluorine (and also *m*-fluorine) resonances can be explained by assuming free rotation of the rings along the Pt−C_{ipso} (C_6F_5) bond. The pattern of the ^{19}F NMR spectrum in acetone-d_6 at room temperature (see Experimental Section) is similar to that seen in $CDCl_3$, but the doublet resonance from J_{F-Tl} is near coalescence, thus suggesting that, in the $[TlPtR_4]^-$ fragment, the dissociation of the Pt−Tl bond is still slow on the NMR time scale even in a donor solvent such as acetone (Scheme 1). When 1 equiv of $TlPF_6$ is added to this acetone-d_6 solution, the Tl···*o*-F is completely lost and only a sharp doublet (δ −113.4, $J_{F-F} \approx 24$ Hz) with platinum satellites ($^3J_{F-Pt} = 256$ Hz) is observed, thus indicating that the presence of additional Tl^I increases the rate of the Pt−Tl dissociation process, although, as expected, the final equilibrium in Scheme 1 seems to be displaced toward the left. Thus, one of the most significant spectroscopic features is the perceptible decrease of the observed $^3J_{o-F-Pt}$ value of about 195 Hz relative to the starting material $(NBu_4)_2[PtR_4]$ (acetone-d_6, δ *o*-F = −113.6 dd, $^3J_{o-F-Pt} = 450$ Hz). This can only be attributed to the formation of the Pt → Tl acceptor bond in the $[TlPtR_4]^-$ fragment that is probably the predominant species in the final equilibrium process (Scheme 1). A similar pattern is observed in the *o*-fluorine region in a mixture of **2** and 1 equiv of $[PtR_4]^{2-}$ in acetone-d_6 (δ −113.5, $J_{F-F} = 28$ Hz), but in this case, the $^3J_{o-F-Pt}$ coupling constant is averaged to a value of 360 Hz in accordance with the higher contribution of the $[PtR_4]^{2-}$ species (final ratio of Pt/Tl is 2:1).

Scheme 1

$$[TlPtR_4]^- \rightleftarrows [PtR4]^{2-} + Tl^+$$

Fluxional behavior is also evident for the trinuclear complex $(NBu_4)_3[Tl\{PtR_4\}_2]$, **1**. Thus, in the *o*-fluorine region, the broad singlet observed at room temperature in $CDCl_3$ (δ −115.2, platinum satellites are not observed)

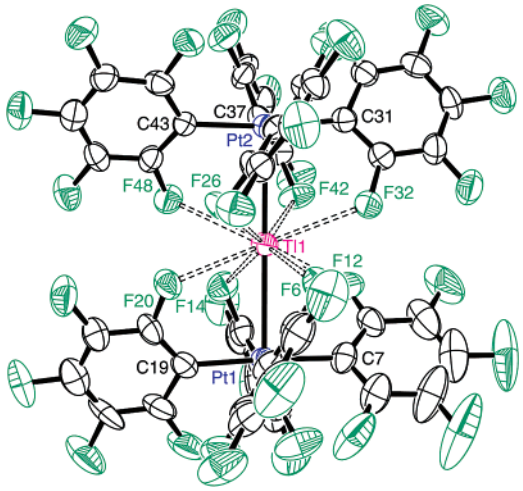

Figure 2. ORTEP view of the anion in $(NBu_4)_3[Tl\{Pt(C_6F_5)_4\}_2]$, **1**. Ellipsoids are drawn at the 50% probability level, showing the arrangement of the aromatic rings and the Tl···F interactions.

coalesces between 243 and 233 K and is resolved in the slow regime (223 K) into the expected two signals: a broad singlet centered at −115.3 ppm, from the exo fluorine atoms, and one extensive broad doublet (δ −115.0) with strong coupling to thallium center ($J_{o-F-^{203,205}Tl} \approx 3530$ Hz), from the endo fluorine atoms. A similar pattern is seen in acetone-d_6 at low temperature (193 K). The loss of the thallium−fluorine coupling at higher temperatures (both in $CDCl_3$ and in acetone-d_6) could be attributed to a very fast dissociation equilibrium between **1** and the homoleptic $(NBu_4)_2[PtR_4]$ starting material. In agreement with this suggestion, the addition of $[PtR_4]^{2-}$ to a $CDCl_3$ solution of **1** results in a ^{19}F NMR spectrum with only one *o*-fluorine resonance (δ −115.3, $^3J_{F-Pt} \approx 375$ Hz). Again, even in the presence of 1 equiv of $(NBu_4)_2[PtR_4]$ (final Pt/Tl ratio 3:1), the observed J_{o-F-Pt} value is still smaller than that in pure $(NBu_4)_2[PtR_4]$.

Crystal Structures. The molecular structures of **1**, **2,** and **3** were confirmed by X-ray crystallographic studies (Figures 2, 3, and 4 and Tables 1 and 2). The structure of the trinuclear *diamagnetic* complex $(NBu_4)_3[Tl\{PtR_4\}_2]$, **1**, can be compared with the analogous and previously reported *paramagnetic* compound $(NBu_4)_2[Tl\{PtR_4\}_2]$, **A**.[11b] Both anions are formed by two square pyramids with a shared apex at the Tl center which is linearly linked to the two platinum atoms of the $[PtR_4]^{2-}$ fragments (Pt−Tl−Pt = 174.01(2) vs 179-(1)° in **A**). In both anions, the two pyramidal basal planes are parallel and almost eclipsed (mean C_{ipso}−Pt···Pt−C_{ipso} = 2.10−4.60° (3.17° average) in **1** vs 2.77° in **A**), and both Pt atoms are slightly shifted from their basal planes toward the Tl atom (0.0884(4) Å for Pt(1) and 0.1033(4) Å for Pt-(2)). The main structural difference between both complexes is found in the Pt−Tl bond distances with slightly different bond lengths in **1** (2.9777(4) and 3.0434(4) Å) which are nearly equal in the paramagnetic complex **A** (2.698(1) and 2.708(1) Å). The bond lengths of the hitherto characterized Pt−Tl[9−12] compounds have been related to the formal oxidation states of the metal ions, being 2.79−3.05 Å for

(22) Bakar, W. A. W. A.; Davidson, J. L.; Lindsell, W. E.; McCullough, K. J.; Muir, K. W. *J. Chem. Soc., Dalton Trans.* **1989**, 991.

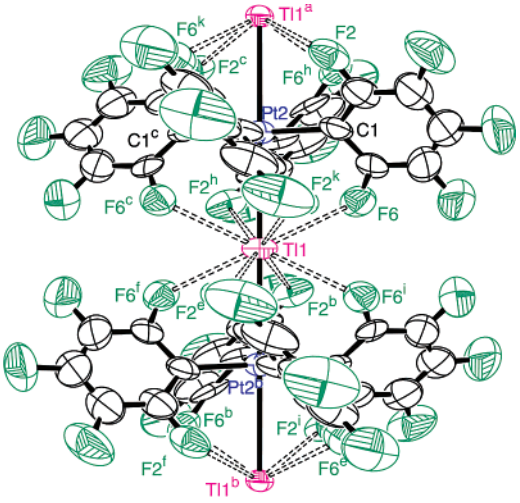

Figure 3. Schematic ORTEP view of part of the chain of the anion in $(NBu_4)_\infty[Tl\{Pt(C_6F_5)_4\}]_\infty$, **2**, showing the arrangement of the aromatic rings and the Tl···F interactions.

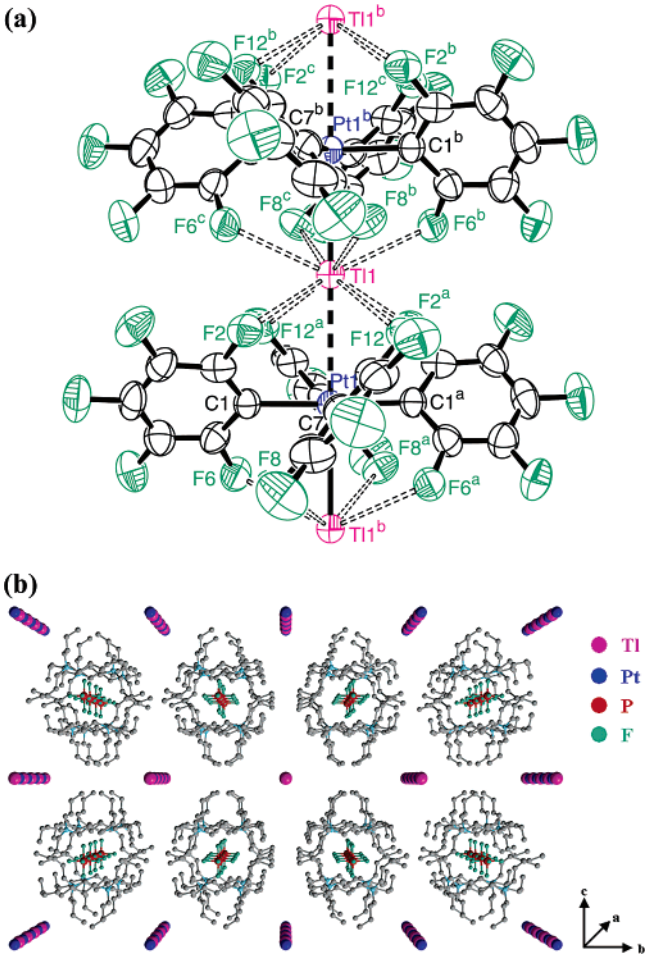

Figure 4. Molecular structure of the anion in $(NBu_4)_\infty[Tl\{Pt(C_6F_5)_4\}]_\infty \cdot \{(NBu_4)PF_6\}_\infty$, **3**. (a) ORTEP drawing with ellipsoids at the 50% probability level of a portion of the polymer chain, showing the arrangement of the aromatic rings and the Tl···F interactions. (b) Unit-cell packing diagram projected down the crystallographic *a* axis.

Pt^0-Tl^I, 2.81−3.14 Å for $Pt^{II}-Tl^I$, and 2.5730−2.638 Å for complexes obtained from reactions of platinum(II) substrates with Tl^{III} ions in which the oxidation states of Pt lay between II and IV and those of Tl are between I and III.[10e−g] Clearly,

Table 2. Selected Bond Distances (Å) and Angles (deg) for $(NBu_4)_3[Tl\{PtR_4\}_2]$, **1**, $(NBu_4)_\infty[Tl\{PtR_4\}]_\infty$, **2**, and $(NBu_4)_\infty[Tl\{PtR_4\}]_\infty \cdot \{(NBu_4)(PF_6)\}_\infty$, **3**

	1	**2**[a]	**3**[b]
Pt−C_{ipso}	2.057(8)−2.085(8)	2.06(2)	2.066(9) 2.077(9)
Pt−Tl	2.9777(4) 3.0434(4)	3.0321(2)	3.1028(6) 3.2306(6)
Tl···F	2.883(5)−2.988(6)	2.956 3.016	2.965(5)−3.060(5)
C_{ipso}−Pt−Tl	88.8(3)−95.5(2)	88.3(6) 91.7(6)	89.2(2)−90.8(2)
Pt−Tl−Pt	174.01(2)	180.0	180.0

[a] Symmetry transformations used to generate equivalent atoms are as follows: #1 $-x+y, -x, z+1/3$; #2 $-x, -x+y, -z+4/3$; #3 $x, x-y, -z+4/3$; #4 $-x, -y, z$; #5 $-y, x-y, z-1/3$; #6 $-x, -y+1, z$; #7 $x, x-y+1, -z+4/3$. [b] Symmetry transformations used to generate equivalent atoms are as follows: #1 $x, -y, -z+1/2$; #2 $x-1/2, y, -z+1/2$; #3 $x+1/2, y, -z+1/2$; #4 $-x+3/2, y, -z$.

the Pt−Tl distances in **1** lie in the expected range, and the observed shortening of about 0.3 Å in complex **A** is remarkable. With reference to previous $d^8-s^2-d^8$ systems involving closed-shell metals, the bonding in the trinuclear Pt_2Tl complex **1** can be qualitatively viewed in light of the orbital diagram resulting from the interaction between the filled $5d_z^2$ (2 Pt) and 6s (Tl) orbitals and the empty set of $6p_z$ orbitals of the three (2 Pt, Tl) metal centers. Mixing of the filled and empty orbitals lowers the energy of all of the filled orbitals giving stability to the $d^8-s^2-d^8$ unit.[6d,e,12g,23] With a similar scheme, the metal core of the paramagnetic complex $(NBu_4)_2[Tl\{PtR_4\}_2]$, **A**, can be viewed as having one less electron than **1** and, thus, an increased bond order of one-half in good agreement with the observed shortening (ca.0.3 Å). Interestingly, the bond distances in $(NBu_4)_2[Tl\{PtR_4\}_2]$, **A** (2.698(1) and 2.708(1) Å) are only slightly longer than those of the famous $[Pt(CN)_4TlL]$ (L = en, DMSO, bipy)[10e−g] complexes reported by Glaser et al. (2.60−2.64 Å), in which the sum of the oxidation states of the two metals is 5, and they are somewhat shorter than the Pt−Tl distances observed in the cationic metallocryptand zerovalent platinum system, $[Pt_2Tl(P_2phen)_3]^+$, reported by Catalano et al. (ca. 2.79 Å).[11c] It is important to note that, as was observed in complex **A**, the Pt−Tl bonds are perpendicular to the planar basal planes (deviation of 2.46 and 1.58°) and the Tl center is surrounded by eight *o*-fluorine atoms (endo atoms), which adopt an antiprismatic disposition (see Figure S1a in Supporting Information) with Tl····F bond contacts (range of 2.883(5)−2.988(6) Å) comparable to those measured in **A** (2.8339(10)−3.065(12) Å). These values are at the low end of the range of Tl····F interactions found (2.98−3.17 Å) in other derivatives,[12b,g,13,22,24] and they are noticeably lower than the sum of the van der Waals radii of Tl and F (3.43 Å).[25] To form these Tl····F contacts, the C_6F_5 rings are oriented toward the same side in both platinum planes,

(23) (a) Ziegler, T.; Nagle, J. K.; Snijders, J. G.; Baerends, E. J. *J. Am. Chem. Soc.* **1989**, *111*, 5631. (b) Dolg, M.; Pyykkö, P.; Runeberg, N. *Inorg. Chem.* **1996**, *35*, 7450.
(24) Han, R.; Ghosh, P.; Desrosiers, P. J.; Trofimenko, S.; Parkin, G. *J. Chem. Soc., Dalton Trans.* **1997**, 3713 and references therein. For a review, see: Plenio, H. *Chem. Rev.* **1997**, *97*, 3363.
(25) Bondi, A. *J. Phys. Chem.* **1964**, *68*, 441.

forming dihedral angles of 54.14−67.88° (61.01° average) with the corresponding platinum coordination planes. The whole coordination of the thallium center (two bonds and eight contacts, see Figures 2 and S1a) does not leave any cleft around the Tl atom, implying that its lone electron pair is stereochemically inactive. This structural feature, usually leading to linear Pt_2Tl entities, has been previously reported,[12c] but significatively, the cationic $Pt_2^{II}-Tl^I$ complex[11a] *cis*-[{$(NH_3)_2Pt(1\text{-}MeT)_2\}_2Tl]^+$ (1-MeT = 1-methylthyminato) displays a bent disposition (Pt−Tl−Pt = 136.7(1) Å) indicative of a stereoactive electron pair at the central Tl^I.

Portions of the heterometallic chains in **2** and **3** are shown in Figures 3 and 4a. In the orange chain (complex **2**), the bimetallic anion $[TlPtR_4]^-$ extends along the *c* axis with uniform Pt−Tl bonds of 3.0321(2) Å. These distances compare well with the Pt−Tl distance (3.0978(2) Å) found in the extended red polymorph of $[Tl^I(C_4H_9N_4)Pt^{II}(CN)_2]$[13b] (3.0256(5) Å in the yellow dimer polymorph). The local geometry at thallium (see Figure S1b in Supporting Information) is similar to that of the trinuclear Pt_2Tl complex **1** being linearly linked to two Pt centers (Tl(1)−Pt(2)−Tl(1a) = 180.0°) and weakly interacting with eight *o*-fluorine atoms (2.956 and 3.016 Å) of the two adjacent PtR_4 units and adopting an antiprismatic disposition. To form these contacts, the C_6F_5 rings are oriented in all planes to the same side, as in complex **1**, but in this case, they rotate counterclockwise forming a dihedral angle of 49.57° with the platinum coordination planes. In contrast, as a consequence of polymerization, two donor−acceptor Pt−Tl bonds are associated with each Pt center in a final pseudooctahedral environment formed by four C_{ipso} atoms from the C_6F_5 groups and the two Tl centers. Alternatively, the chain can be viewed as a columnar stack of parallel PtR_4 fragments connected through equivalent thallium centers (average torsion angle $C_{ipso}-Pt\cdots\cdots Pt-C_{ipso}$ = 30°).

As was mentioned above, slow crystallization of a solution of $(NBu_4)_2[PtR_4]$ and $TlPF_6$ (1 equiv) in EtOH resulted in the isolation of greenish-yellow needles of a new product, **3**, which was characterized as an adduct of complex **2** and the resulting $(NBu_4)(PF_6)$ salt. As shown in Figure 4a, complex **3** involves a somewhat novel 1D Pt−Tl mixed chain. The most striking structural feature, induced by the co-deposition of the $(NBu_4)(PF_6)$ salt, was the breakdown of the regular Pt···Tl bond separation observed in **2**. In this case, the interaction of the Tl centers with the two adjacent $[PtR_4]$ fragments is asymmetric, and as a consequence, two different contacts, one shorter (3.1028(6) Å) and the other longer (3.2306(6) Å), are present in the chain. Both distances are effectively longer than the Pt−Tl bond separation of 3.0321(2) Å in **2**. The shortest distance Pt(1)−Tl(1b) (3.1028(6) Å) is in the usual range for $Pt^{II}-Tl^I$ separations found in other compounds (2.81−3.14 Å). However, the longest one, 3.2306(6) Å, which is shorter than the sum of the van der Waals radii (3.68 Å), lies out of the usual range of $Pt^{II}\cdots Tl^I$ bond distances, suggesting that the attractive interactions between consecutive discrete bimetallic anionic $[TlPtR_4]^-$ fragments is weaker. This Pt····Tl separation compares to that recently reported in the trinuclear complex $[(c\text{-}C_5H_9)_{14}Si_{14}O_{18}(O\text{-}SiMe_3)_2O_4(COD)PtTl_2]$[11e] (3.2393(15) Å). Although the angles at the metal centers (180.0°) and the thallium−*o*-fluorine contacts (2.965(5)−3.060(5) Å) are similar to those observed in **1** and **2**, in this complex, the eight fluorine atoms that contact the Tl center adopt a slightly distorted cubic environment (see Figure S1c in Supporting Information). As a consequence (see Figure 4a), the C_6F_5 rings are now tilted in consecutive coordination planes to opposite sides, forming dihedral angles of 49.93−52.98° (51.46° average) with the platinum planes. The F···Tl contacts facilitate the link between adjacent $[TlPtR_4]^-$ units, thus contributing to the stabilization of the final chain ($C_{ipso}-Pt-Pt-C_{ipso}$ = 21.6−22.5°, 22.05° average). As is observed in Figure 4b, which shows a small portion of the extended crystal packing, each PF_6^- anion is surrounded by four cations and resides inside the channels formed by the mixed-metal anionic columns. The columnar structure has long separations between the thallium (or platinum) atoms of different chains (Tl···Tl (or Pt···Pt) = 14.294 and 17.843 Å, along the *b* and *c* axes, respectively).

Photophysical Properties. Dissolution of the crystals of complexes **2** (orange) and **3** (greenish-yellow) in solvents such as CH_2Cl_2, acetone, or acetonitrile ($\sim 2 \times 10^{-5}$ M) led to a loss of their colors, yielding colorless solutions, indicating that the color comes from solid-state effects. The room-temperature absorption spectra of the three complexes (**1**−**3**) are essentially identical (See Figure S2 in Supporting Information). A low-energy absorption at 350 nm, which is absent in the precursor, seems to be characteristic of the presence in solution of the $[TlPtR_4]^-$ system and, on the basis of previous assignments in d^8-Tl^I systems,[6d,9,10a,12g,26] is tentatively attributed to a spin- and symmetry-allowed $\sigma^*-\sigma$ system with some metal-to-metal (Pt−to−Tl) charge-transfer (MM′CT) character.[6d,12g,23] In the solid state, the Pt···Tl bonding contacts in both 1D chain complexes (**2** and **3**) are observed as a broad absorption, spanning the range from ca. 375 to 700 nm (Supporting Information, Figure S3). The remarkable difference in the absorption maxima (488 nm for **2** vs 410 nm for **3**) is attributed to the larger Pt···Tl separation in **2** (3.0321(2) Å) relative to that in **3** (3.1028(6) and 3.2306(6) Å). We noted that when crystals of the trimetallic complex $(NBu_4)_3[R_4Pt\text{-}Tl\text{-}PtR_4]$, **1**, are crushed and ground, a visual change from white to pale yellow is observed. This fact also causes a perceptible change in the luminescence, from bright blue to bright green, under illumination with UV radiation.

Although the presence of Pt−Tl bonds is often associated with luminescent properties, several bi- and trinuclear compounds containing Tl^I coordinated to Pt^0 or Pt^{II} have been found to be nonemissive.[10c,11a] Complexes **1**−**3** offer us the opportunity to compare the behavior of this polar metal−metal bond in different electronic situations. The photophysical data are collected in Table S1, and selected spectra are shown in Figures 5 and 6 and S4−S7.

As is observed in Figure 5, in the solid state at room temperature, the white crystalline solid of the trinuclear anionic complex **1** produces an intense blue luminescence (λ_{max} = 450 nm) with excitation at 345−350 nm, which can

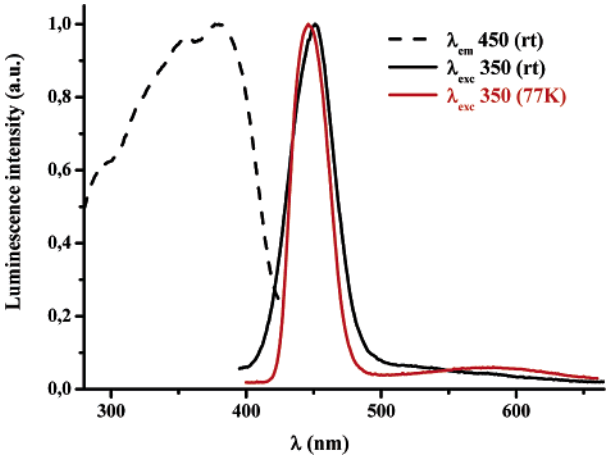

Figure 5. Normalized excitation and emission spectra of $(NBu_4)_3[Tl\{PtR_4\}_2]$, **1**, in solid state (powder) at room temperature and at 77 K.

be compared to that previously reported for the neutral $[Tl_2Pt(CN)_4]$ (solid 300 K, 448 nm, $\tau = 0.25$ μs)[9a] and cationic $[Tl(crown\text{-}P_2)Pt(CN)_2](NO_3)$ (CH_2Cl_2, 451 nm)[10a] complexes, respectively. This emission band, related to two excitation profiles at ca. 350 and 385 nm and with an emission lifetime typical of triplet multiplicity (10.2 μs), is essentially not dependent on the temperature (77 K, $\lambda_{max} = 445$, $\tau = 12.1$ μs) and on the excitation wavelength. The slight increase in the lifetime upon cooling is consistent with a reduction in the nonradiative decay rate. In contrast, the emission and the lifetime of the related $[Tl_2Pt(CN)_4]$ complex reported by Balch and co-workers[9] are temperature dependent. In particular, the lifetime lengthens considerably at lower temperatures (1.4 μs, 77 K; 77 μs, 1.4 K),[9b] and at $\leq$77 K, a second emission red band clearly resolves (at 1.4 K, two bands at 457 and 577 nm were observed).[9b] On the basis of previous assignments, the emission in **1** is attributed to the Pt−Tl chromophore and assigned to a MM′CT transition. Curiously, when the luminescence spectrum is recorded in KBr pellets, it displays two independent emissions associated with different excitation profiles at 465 and 532 nm (See Figure S4, Supporting Information). As previously commented, the color of the powder (white to pale yellow) and the luminescence changes slightly upon crushing and grinding of the sample, a process that would probably favor the presence of different cromophores with shorter Pt···Tl interactions. The room-temperature colorless solutions of **1** in CH_2Cl_2 or acetone (2×10^{-5} or 10^{-3} M) are not luminescent. However, upon freezing in a liquid N_2 bath, these solutions become intensely luminescent, and it was noted that the most concentrated glasses (10^{-3} M) are pale yellow in color. The spectra in acetone show several bands in the range of 420−590 nm whose intensities are dependent on the concentration and excitation wavelength. Similar behavior is observed in the CH_2Cl_2 glass (four maxima at 438, 484, 530 max and 595 sh are seen with a solution of 2×10^{-5} M), but in this solvent, the high-energy bands are not observed at higher concentrations (one or two broad emissions in the range of 520−660 nm are seen, which are found to be wavelength dependent). It is interesting to note that in both solvents some frozen-solution emission bands are red-shifted beyond the solid state-emission seen in Figure 5. This behavior is not common, but it is not unprecedented.[3k−m] As has been previously noted in other d^{10} systems,[3k−m] the process of freezing the solution probably causes the formation of different aggregates of the $[Pt-Tl]_n$ or $Pt-[Tl-Pt]_n$ type, or perhaps excimers or exciplexes with different degrees of Pt···Tl interactions in the various glasses, which could be responsible for the observed luminescence, although interaction with solvent molecules cannot be excluded.

The photoluminescence emission spectra at different temperatures of **2** and **3** are shown in Figure 6. A polycrystalline sample of **2** (Figure 6a), with a regular short Pt−Tl separation, displays, regardless of the excitation wavelength, an intense orange luminescence ($\lambda_{max} = 582$ nm) with a monoexponential decay of 11.6 μs; the luminescence becomes red at 77 K. The red emission at 77 K has two bands, an intense red peak at 635 nm ($\tau = 12.6$ μs) and a small orange shoulder at 575 nm ($\tau = 10.4$ μs). The excitation profile of both bands, showing a sharp edge located at ca. 550 nm, is identical, and the lifetimes are similar, suggesting that both bands are in a thermal equilibrium or correspond to different sublevels of the same emitting triplet excited state. The large shift of the emission maximum from the trinuclear complex **1** to **2** suggests a strong perturbation due to the formation of the chain in which the discrete orbital levels are replaced by bands, as has been previously reported for platinum-chain metal systems.[4a,b,27] In **2**, the consecutive Pt···Tl interactions produce bands with a small energy gap between the last filled band and the lowest empty one, which should clearly lower the energy of the emission. The red shift upon cooling (582 → 635 nm) is consistent with a decrease in the metal−metal separation caused by thermal contraction, a phenomenon that has many precedents in extended chain systems.[4a,b,27] As mentioned in the Introduction, the formation of an extended Pt···Tl···Pt···Tl chain in the red polymorph of $[Tl^{I}(C_4H_9N_4)Pt^{II}(CN)_2]$ has been recently reported, but no emissive properties were reported.[13b] By comparison, in related gold−thallium chain systems, the lifetimes were usually shorter (i.e., $\{AuTl[Ph_2P(CH_2)S]_2\}_\infty$[3n], $\lambda_{em} = 565$ nm, $\tau = 0.98$ μs, 298 K; $[TlAu(C_6Cl_5)]_\infty$[3i], $\lambda_{em} = 531$ nm, $\tau = 1$, 0.1 μs).

As is shown in Figure 6b, in adduct **3**, the disruption in the chain caused by the presence of $(NBu_4)(PF_6)$ results in a remarkable blue shift in the energy of the emission from orange ($\lambda_{max} = 582$ nm) in **2** to green ($\lambda_{max} = 505$ nm) in **3** and in the excitation spectrum, which in this adduct has a less-sharp edge located at ca. 440 nm. For product **3**, the emission shifts to lower energies and increases its intensity upon lowering of the temperature (77 K, 524 nm), thus indicating that there is a thermally activated nonradiative decay pathway that is less significant at lower temperatures. As can be observed, a less-intense high-energy band at 446 nm also develops at temperatures below ~230 K. The emission decay observed for the intense low-energy band was monoexponential, and the values (13.7 μs, 298 K; 14.2 μs, 77 K) suggest that the emission originates from a state of triplet multiplicity. Interestingly, the color of **3** changes from greenish-yellow to pale orange upon the crushing and

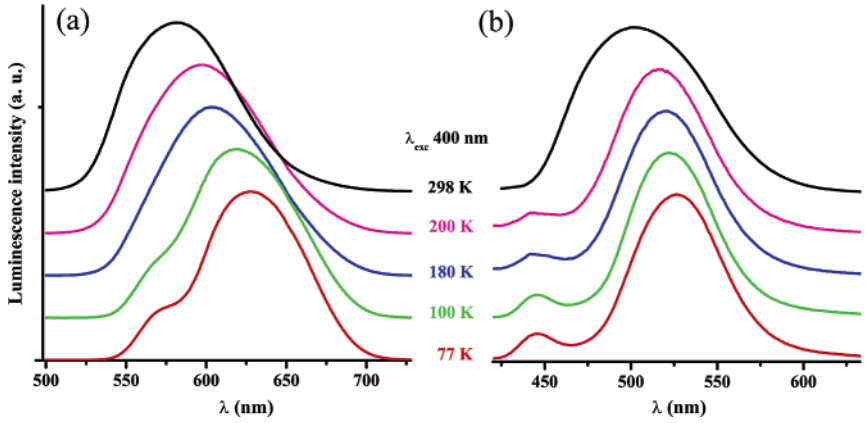

Figure 6. Variable-temperature normalized emission spectra of (a) $(NBu_4)_\infty[Tl\{PtR_4\}]_\infty$, **2**, and (b) $(NBu_4)_\infty[Tl\{PtR_4\}]_\infty\cdot\{(NBu_4)(PF_6)\}_\infty$, **3**, in the solid state (powder).

grinding of the microcrystalline sample, and in fact, the luminescence spectrum of a sample (KBr pellet) prepared using a pressure of 10 Torr for 5 h shows a maximum (582 nm, λ_{exc} = 390−520 nm) that is very close to that observed for complex **2** (590 nm in KBr, 582 nm in solid powder). However, the emission spectra of **3** in KBr pellets, prepared in the usual way (∼5 min), depend on the excitation wavelength (see Figure S5 in Supporting Information), suggesting the presence of multiple emissions that could be tentatively attributed to the formation, under pressure, of different chromophores, $[TlPtR_4]_x$, with a distribution of Pt−Tl contacts emitting in a close range of energies.

Products **2** and **3** are not emissive in fluid solutions (CH_2Cl_2 or acetone) but bright luminescence is seen when the solutions are frozen. Not surprisingly, the color and the emissions are dependent on the solvent concentration and excitation wavelength, and they also exhibit thermochromism (see Table S1). For example, a frozen (77 K) CH_2Cl_2 or acetone solution of complex **2** changes color from purple (10^{-3} M) to red (10^{-4} M), finally vanishing to pale cream when it is diluted to 2×10^{-5} M. Similar behavior is observed for **3**. Thermochromism is also evident when 77 K samples of **2** and **3** are allowed to warm slowly. An initial frozen sample of **3** in acetone (10^{-3} M), for example, changes progressively from dark purple to red and orange before eventually becoming colorless upon warming. In both products, frozen concentrated solutions (10^{-3} M) display a broad low-energy band (**2** 740 nm (*acetone*, λ_{exc} = 470−600 nm), 700−710 nm (*CH_2Cl_2*, λ_{exc} = 500−600 nm); **3** ca. 730 (*acetone*, λ_{exc} = 500−600 nm), 690 (*CH_2Cl_2*, λ_{exc} =420−600 nm)) whose maximum is only slightly dependent on the excitation wavelength. Upon dilution, high-energy emissions are observed (**2** *acetone* 430, 455, 480, 535 nm (2×10^{-5} M), 430, 480, 550, 655 nm (10^{-4} M); *CH_2Cl_2* 523, 604 nm (2×10^{-5} M), 645−700 (10^{-4} M); **3** *acetone* 424, 438, 480, 530, 545 nm (2×10^{-5} M); *CH_2Cl_2* 635−690 nm (2×10^{-5} M)), the intensities of which are dependent on the wavelength used for excitation. As an illustration of this, the emission spectra of **2** at concentrations of 10^{-4} M and 2×10^{-5} M and at several excitation wavelengths are shown in Figures S6 and S7 in the Supporting Information. Once again, the freezing process may create an array of specific aggregates. The different emission bands, the colors, and the thermochromism observed in frozen glass media at different concentrations probably result from changes both in the size of the aggregates formed, based on Pt···Tl contacts, and the specific Pt···Tl distance within the fragment or aggregate. As was expected, the formation of extended aggregates emitting at even lower energies than solid **2** is favored in the most concentrated solutions (10^{-3} M). The high energy emissions at ca. 430 and 455 nm (the latter at a energy similar to that seen for solid **1**), are tentatively attributed to the presence of discrete $[TlPtR_4]^-$ and $[Tl\{PtR_4\}_2]^{3-}$ fragments, respectively. Alternatively, the *concentration luminochromism* leading to multiple emissions could also be related to different extents of excited-state association of $[TlPtR_4]$ fragments, the emitting species in solution being $*[TlPtR_4]_x$ oligomeric excimers and exciplexes. Similar assignments have already been given by Patterson and co-workers for the excited-state oligomerization of $[M(CN)_2]^-$ (M = Cu, Ag)[3l] or more recently by Omary et al. to explain the luminescence properties of trinuclear copper(I) pyrazolates.[3m] However, in this platinum−thallium system (1:1 Pt/Tl ratio, complexes **2** and **3**), the dramatic color changes usually observed upon cooling are suggestive of ground-state oligomerization.

In conclusion, the formation, structure, and spectroscopic and photophysical behavior of $(NBu_4)_3[Tl\{PtR_4\}_2]$, **1**, $(NBu_4)_\infty[Tl\{PtR_4\}]_\infty$, **2**, and $(NBu_4)_\infty[Tl\{PtR_4\}]_\infty\cdot\{(NBu_4)(PF_6)\}_\infty$, **3**, have been described. While in **1** a Tl center is sandwiched by two $Pt(C_6F_5)_4^{2-}$ fragments and each Pt center forms only one Pt−Tl bond, in **2** both the Tl^I and the Pt^{II} centers are involved in two short Pt−Tl bonds leading to an extended linear-chain system. It should be noted that even in the presence of a large excess of Tl^I, no evidence of the formation of a neutral trimetallic entity, Tl_2PtR_4, has been found. This fact contrasts with the behavior of other dianionic platinate(II) fragments such as $[Pt(CN)_4]^{2-}$[9] and *cis*- or *trans*-$[Pt(C_6F_5)_2(C{\equiv}CR)_2]^{2-}$.[12g,13a] In presence of $(NBu_4)(PF_6)$, the $TlPF_6/(NBu_4)_2[PtR_4]$ system generates adduct **3** containing a novel chain which is formed by discrete $[TlPtR_4]^-$ fragments connected through additional weaker Tl···Pt bonding contacts. The disruption of the chain in **2** caused by the presence of $(NBu_4)(PF_6)$ has some resemblance to

the well-known influence of the size of the counterion in the stacked 1D cationic square planar platinum structures.[28,29] In fluid solution, the Pt···Tl bonding interactions seem to be partially broken but association occurs easily in frozen glasses as noted by the presence of multiple emissions probably resulting from a distribution of different aggregates, which are solvent and concentration dependent. Current efforts are focused on the study of the behavior of other dianionic mixed platinate systems such as $[Pt(C_6F_5)_y(CN)_x]^{2-}$ ($x, y = 1-3$) toward Tl(I). Examination of their photophysical properties as well as theoretical studies will provide insight into the nature of the Pt(II)−Tl(I) interaction and its relationship with the observed photoluminescence.

Acknowledgment. This work is dedicated to Prof. Victor Riera on the occasion of his 70th birthday. We thank the Dirección General de Investigación of Spain (Projects BQU2002-03997-C02-01, 02, CTQ2005-08606-C02-01, and CTQ2005-03141 and a grant for A.G.).

Supporting Information Available: Table of photophysical data (Table S1), Figures S1−S7, and crystallographic data in CIF format. This material is available free of charge via the Internet at http://pubs.acs.org.

IC051818U

(26) Balch, A. L.; Neve, F.; Olmstead, M. M. *J. Am. Chem. Soc.* **1991**, *113*, 2995.
(27) Zheng, G. Y.; Rillema, D. P. *Inorg. Chem.* **1998**, *37*, 1392 and references therein.
(28) The more common structural types in one-dimensional extended platinum(II) systems are linear chains with a single Pt···Pt distance and dimer structures in which the platinum chain segregates into pairs exhibiting a short and a long separation. The precise structure is sensitive to different electronic and steric factors and also to the size of the counterion (assuming the complex is ionic). See ref 4b
(29) Yam, V. W.-W.; Chan, K. H.-Y.; Wong, K. M.-C.; Zhu, N. *Chem.—Eur. J.* **2005**, *11*, 4535 and references therein.